16th World Conference on Earthquake, 16WCEE 2017

Santiago Chile, January 9th to 13th 2017

Paper N° 4615

Registration Code: S- V1464679719

PROBABILISTIC SEISMIC RISK ASSESSMENT OF CONTINUOUS STEEL PIPELINES FOR FAULT OFFSET BY MONTE CARLO SIMULATIONS

S. Akkar[(1)], Y. Cheng[(2)]

[(1)] *Professor, Kandilli Observatory and Earthquake Engineerin, Bogazici University - Turkey, sinan.akkar@boun.edu.tr*
[(2)] *Postdoctoral fellow, Kandilli Observatory and Earthquake Engineerin, Bogazici University - Turke, yin.cheng@boun.edu.tr*

Abstract

Buried continuous steel pipelines are commonly used as reliable and economic means to transport oil and gas across the world. Such pipelines generally cover long distances and their exposure to the earthquakes while crossing active faults in earthquake-prone regions cannot be overlooked at the design stage. The mechanical properties of the material used in continuous steel pipes make them insensitive to dynamic ground motions intensity measures such as PGA and PGV. However, they are vulnerable to permanent fault offset (displacements) at fault crossings that should be considered in their design. This study presents a full probabilistic risk assessment of pipeline failure at fault crossings through hazard to risk. In order to achieve the probabilistic risk evaluation, the seismic hazard assessment of fault displacement using proposed Monte-Carlo simulation is first introduced. Then the proposed theory of the risk assessment is implemented to the case studies that focus on strike-slip fault crossings. Two uncertainties from the earthquakes, i.e., fault displacement and fault-pipe crossing angles, are considered in the probabilistic risk assessment. The influence of these uncertainties in the risk of pipe failure is evaluated. The seismic risk of pipeline failure due to the actual fault rupture occurring at a distance far away from the mapped fault trace is additionally examined in the case studies. The probabilistic risk presented in the paper can be a useful reference for engineers to design and retrofit continuous pipes at fault crossings.

Keywords: probabilistic permanent fault displacement hazard; Monte Carlo simulation; probabilistic continuous pipeline risk; continuous pipeline seismic design

1. Introduction

Buried continuous steel pipelines are commonly used for transporting oil and gas across the world. They generally cover long distances and their exposure to the earthquake threats while crossing seismically active faults cannot be overlooked at the design stage. Unlike water pipelines, which are generally constructed as segmented pipes, the continuous steel pipelines are more likely to suffer damage due to permanent fault displacements (PFDs) rather than ground strains caused by seismic wave propagation. The 1971 San Fernando, 1994 Northridge, 1999 Kocaeli and 2001 Alaska earthquakes caused serious continuous pipeline damages at fault crossings with human casualties and economic losses. Therefore, reliable seismic hazard and risk assessment of continuous pipelines at fault crossings is important to mobilize the most efficient design and retrofitting techniques for earthquake induced risk mitigation.

When a continuous pipeline is subjected to surface fault rupture, the resulting stresses along the pipeline are complicated because they depend on many factors such as style-of-faulting, pipe material, pipe dimensions (thickness and diameter), pipe alignment with respect to fault strike and soil property surrounding the pipe. There are numerous studies in the literature that investigate the mechanical behavior of a pipeline at fault crossings (e.g. [13-18]). The results of these studies do not consider the earthquake originated uncertainties that may affect the damage state in the continuous buried pipelines. The probabilistic seismic risk analysis of buried pipelines are focused on segmented pipelines (e.g. [1-6]) by using empirical fragility functions that relate ground shaking (e.g. [7-10]) or ground strain (e.g. [11-12]) to repair rate. (Geographically distributed segmented pipelines are vulnerable to transient ground shaking). Therefore, probabilistic failure due to fault crossings (i.e., PFDs) critical to continuous steel pipelines is yet to be investigated in sufficient details.

Recent developments in probabilistic PFD hazard [19-21], however, provide good basis to implement probabilistic seismic risk assessment to continuous pipelines. Understanding the probabilistic risk of pipelines at different earthquake levels would be important to the pipeline operator to take necessary actions for mitigating seismic pipeline vulnerability.

This study presents the theory and application of probabilistic seismic risk assessment of buried continuous steel pipelines induced by PFD. The probabilistic PFD is computed via Monte Carlo (MC) simulations and probabilistic risk is represented by the expected annual exceedance rate of pipeline failure. The paper first introduces the MC-based hazard assessment method (theory and application) to model probabilistic PFD. This is followed by the discussions on probabilistic risk assessment of pipeline failure triggered by PFD. The presented case studies facilitate the understanding of these concepts and also show the significance of uncertainties resulting from the intrinsic nature of earthquake process as well as pipeline mechanical behavior. The complexities in earthquake rupture are accounted for by mapping accuracy of faults and complexity of fault rupture that would results in variations in the relative locations of ruptured fault and pipe. The mechanical behavior of pipe is constrained to pipe cross-section dimension, soil properties surrounding the buried pipe, buried depth of pipe and variations in pipe-fault crossing angle. The observations from the presented case studies are discussed within the context of design and risk assessment regulations enforced by current continuous pipeline design guidelines.

2. Methodology

2.1 Monte-Carlo based probabilistic hazard for PFD

The current state-of-practice (e.g., pipeline designs codes) tends to estimate PFDs deterministically from empirical surface rupture vs. magnitude relationships (e.g. [22]). Alternative to this approach, Youngs et al. [20] developed the probabilistic fault displacement hazard assessment (PFDHA) for the Yucca Mountain Nuclear Waste Repository Project for normal faults to expresses the annual exceedance rates of fault displacements at different thresholds. The methodology is inspired from conventional probabilistic seismic hazard assessment (PSHA). It is further studied in Petersen et al. [21] for strike-slip faults by including the mapping accuracy and ruptured fault complexity. Our method uses the Petersen et al. model and it considers the likely occurrence of

on-fault (D) and off-fault (d) displacements. The former displacement occurs on the major ruptured fault and the latter displacement typically represents discontinuous shear-failures at locations far from the principal fault.

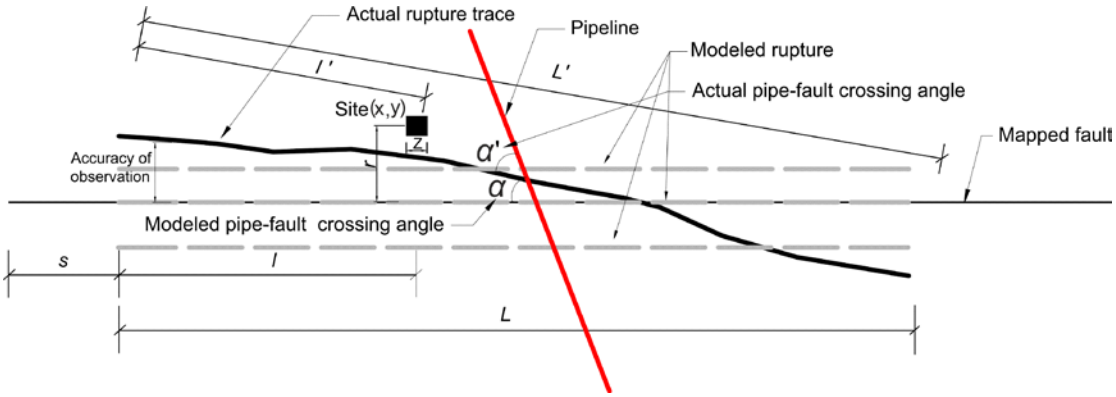

Fig. 1 Modeled and actual fault layout for Petersen et al. [21] PFDHA approach for strike-slipe earthquakes. The *accuracy of observation* represents the combined effects of fault mapping accuracy and rupture complexity on the *modeled* and *actual* rupture conditions.

Our interpretations of ruptured fault segment and site geometry used in Petersen et al. [21] are presented in Figure 1. The plot shows the *modeled* and *actual* fault layout. The *modeled* configuration is used in PFDHA by incorporating the uncertainties due to mapping inaccuracy and complexity of fault rupture. The site is represented as a square cell having a dimension of z and x, y denote the coordinates of the center of the site. Fault distance, r, is the perpendicular distance from the *modeled* rupture length, L. l denotes the distance between the closest end to the nearest point on the *modeled* rupture. s is the distance from the end of the *modeled* rupture to the end of the *modeled* fault. We mimic the potential deviations in the rupture from the mapped (*modeled*) fault trace by introducing offsets normal to the strike of the mapped fault. Petersen et al [21] describe these offsets with a set of standard deviations (Tables 2 and 3 in [21] at fault crossings) for different categories of mapping accuracy (accurate, approximate, concealed and inferred) and fault complexity (simple or complex). L' and l' are the counterparts of L and l, respectively. They also address the uncertainty in the relative positions of rupture and site due to intricate variations in fault rupture conditions.

Equations (1) and (2) show the annual exceedance rates of on-fault $\gamma(D \geq D_0)$ and off-fault $\gamma(d \geq d_0)$ displacements that are given in Petersen et al. [21].

$$\gamma(D\geq D_0)=\nu_{\min}\int_{m,s} f_{M,S}\,(\mathrm{m,s})P[sr\neq 0|m]\int_r P[D\neq 0|z,sr\neq 0]\times P[D\geq D_0\,|l/L,m,D\neq 0]f_{l/L}\,(l/L)f_R\,(r)\mathrm{d}(l/L)\mathrm{d}r\mathrm{d}m\mathrm{d}s \quad (1)$$

$$\gamma(d\geq d_0)=\nu_{\min}\int_{m,s} f_{M,S}\,(\mathrm{m,s})P[sr\neq 0|m]\int_r P[d\neq 0|r,z,sr\neq 0]\times P[d\geq d_0\,|r,m,d\neq 0]\,f_R\,(r)\,\mathrm{d}r\mathrm{d}m\mathrm{d}s \quad (2)$$

The probabilistic terms in Equation (1) include (a) the uncertainty in rupture location due to random variation of rupture along the fault as well as the fault complexity and mapping inaccuracy, $f(r)$; (b) the joint probability to characterize the relation between earthquake magnitude (m) and rupture location (s), $f_{M,S}(m,s)$; (c) the probability of observing surface rupture (sr) conditioned on earthquake magnitude, $P(sr \neq 0|_m)$; (d) given a nonzero surface rupture the probability of observing a nonzero on-fault displacement at a site of dimension z, $P(D \neq 0|_{z,\, sr \neq 0})$ and (e) the probability of on-fault displacement exceeding a threshold D_0 conditioned on rupture geometry and earthquake size. The last conditional probability is lognormal and is developed from an on-fault empirical displacement predictive model (on-fault displacement GMPE). Apart from these probabilistic terms, the minimum rate, ν_{min}, constrains the frequency of earthquake occurrence in the model. It is a function of magnitude and can be a single rupture rate or can be a function of cumulative earthquakes above a minimum magnitude of engineering significance (Youngs et al. [20]).

The probabilistic terms that describe the annual exceedance rate of off-fault displacements $\gamma(d \geq d_0)$ show some similarities with Equation (1). In fact, the first three probabilities defined in $\gamma(D \geq D_0)$ also exist in $\gamma(d \geq d_0)$. In the computation of $\gamma(d \geq d_0)$, the probability of nonzero off-fault displacement given a nonzero surface rupture $[P(d \neq 0|_{r,\, z,\, sr \neq 0})]$ not only depends on the size of the site (z) but also on the perpendicular distance, r, between the site and the rupture. This is because the discontinuous off-fault displacements are expected to occur

away from the fault due to shears and fractures in the vicinity of principle rupture. The empirical GMPE to describe the probability of off-fault displacement exceeding a threshold d_0 [$P(d \geq d_0|_{r,\, m,\, d \neq 0})$] is a function of r and m for $\gamma(d \geq d_0)$. The reader is referred to Petersen et al. (2011) and Youngs et al. [20] for details of conventional probabilistic fault displacement hazard integral. The next paragraph explains the integration of these probabilities to MC-based PFD hazard.

Our MC-based PFD hazard assessment starts with the generation of synthetic earthquake catalogs to reflect the temporal seismicity of the subject fault. The procedure of generating synthetic catalogs is already given in Akkar and Cheng [23]. Each synthetic catalog contains a series of events that follows the designated magnitude recurrence model within the predefined catalog period. For each event in the synthetic catalog, Figure 2 shows the proposed procedure to generate probabilistic on-fault and off-fault displacements at the centroids of the cells covered by the region of interest. The grid size is z and it varies from 25 m to 200 m in Petersen et al. [21] to account for different levels of accuracy in rupture probability. The mesh gridding is done only within several hundred meters (e.g., 150 m) from each side of the fault because fault displacements decay rapidly with increasing distance from the ruptured fault segment.

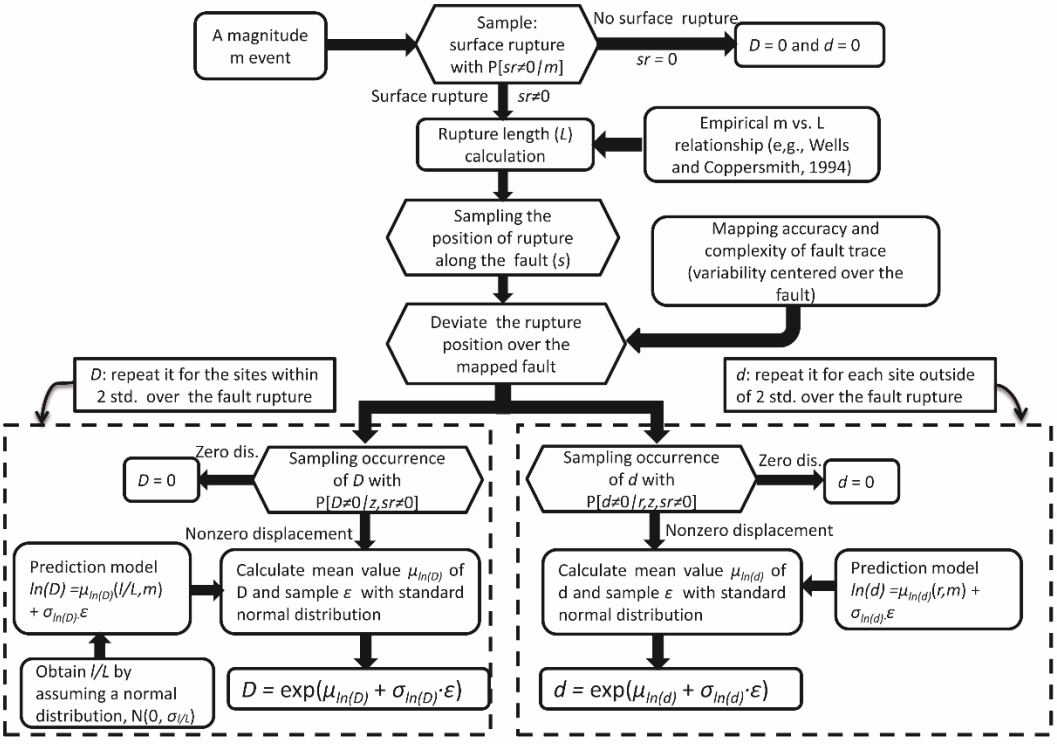

Fig. 2 Proposed MC-based permanent fault displacement hazard assessment procedure

We first compute the conditional probability of observing surface rupture on the fault, $P(sr \neq 0|_m)$, for each scenario event with a designated magnitude m in the earthquake catalog (Equation (3)).

$$P(sr \neq 0|m) = e^{-12.51+2.053m}/(1+e^{-12.51+2.053m}) \quad (3)$$

The conditional probability follows Bernoulli distribution that samples the "success" ($sr \neq 0$) or "failure" ($sr = 0$) of a random event under the computed probability given in Equation (3). If Bernoulli distribution samples "failure", both on- and off-fault displacements are zero for that scenario event. If the earthquake with surface rupture is sampled, an empirical m vs. L scaling relationship is used (e.g. [22]) to determine the rupture length, L. The rupture position (s) is randomly placed along the entire fault assuming a uniform distribution. The likely deviation in the rupture location from the mapped fault trace due to mapping uncertainty is determined from a two-sided normal probability distribution proposed by Petersen et al. [21]. (See Table 2 in the referred article). After determining the final location of the ruptured segment, the on- and off-fault displacements are

generated as given in the dashed boxes in Figure 2. The random generation of on- and off-fault displacements start with the consideration of probabilities $P(D \neq 0|_{z,\ sr \neq 0})$ and $P(d \neq 0|_{r,\ z,\ sr \neq 0})$. These probabilities are expressed as power functions and are given in a tabular format in Petersen et al. [21] for different grid sizes. They also follow Bernoulli distribution and if the Bernoulli distribution samples "failure" for any one of these probabilities, the corresponding fault displacement is taken as zero. (In practice, $P(D \neq 0|_{z,\ sr \neq 0})$ can be taken as unity and Bernoulli distribution samples "success" whenever a non-zero surface rupture is generated). Otherwise, the on- and off-fault displacements are estimated from the proposed empirical GMPEs by Petersen et al. [21]. The generic forms of these GMPEs are given in Equations (4) and (5).

$$\ln(D) = \mu_{\ln(D)}\ (l/L,\ m) + \varepsilon \cdot \sigma_{\ln(D)} \tag{4}$$

$$\ln(d) = \mu_{\ln(d)}\ (r,\ m) + \varepsilon \cdot \sigma_{\ln(d)} \tag{5}$$

$\mu_{\ln(D)}$ and $\mu_{\ln(d)}$ are the logarithmic mean estimates of on- and off-fault displacements, respectively. $\sigma_{\ln(D)}$ and $\sigma_{\ln(d)}$ describe the logarithmic standard deviations associated with the on- and off-fault displacement GMPEs, respectively. ε designates the number of standard deviations above or below the logarithmic mean estimates. Consistent with the conventional wisdom in GMPEs, D and d are log-normal varieties whereas ε is normally distributed in the above expressions. Petersen et al. [21] propose three alternative prediction equations to estimate on-fault displacements depending on the observed data from the past strike-slip earthquakes. These equations are strictly valid for on-fault sites (cells) after considering the mapping uncertainty and fault complexity while determining the location of ruptured segment on the principal fault. We treat l/L as a normal variate to consider the uncertainty between the relative positions of rupture and site locations resulting from complexities in rupture process. The off-fault displacement predictive model is used at the sites (cells) encircling the major ruptured fault segment. The off-fault sites are only within few hundred meters from both sides of the ruptured fault segment due to rapid decay of fault displacements with distance.

The algorithm given in Figure 2 is repeated for all the earthquakes in the generated synthetic catalogs to compute the on- and off-fault displacement distributions at the centroid of each cell. The annual exceedance rates of on-fault and off-fault displacements at each cell for predefined threshold levels are determined from the following expressions:

$\lambda_j\ (D \geq D_0)$ = (total number of $D \geq D_0$ at site j)/(total number of simulated earthquake catalogs × catalog period) (6)

$\lambda_j\ (d \geq d_0)$ = (total number of $d \geq d_0$ at site j)/(total number of simulated earthquake catalogs × catalog period) (7)

In Equations (6) and (7) j refers to the cell index whereas D_0 and d_0 are the threshold on-fault and off-fault displacements, respectively. The on-fault and off-fault displacement hazard curves at cell j are obtained from the computation of $\lambda_j(D \geq D_0)$ and $\lambda_j(d \geq d_0)$ for a set of D_0 and d_0, respectively. The total permanent displacement hazard curve at cell j is the sum of on- and off-fault hazard curves corresponding to cell j.

2.2 Probabilistic seismic risk assessment of pipelines due to PFD

The pipeline seismic risk against faults rupturing at the surface is represented by the annual exceedance rate of pipeline failure. This is achieved by integrating the probabilistic fault displacement hazard, mechanical response of pipe due to fault displacement and empirical pipe fragility function. The concept is similar to the conventional probabilistic seismic risk assessment [24]. Since both tensile and compressive strains developed along the pipe during an earthquake can cause pipe's failure, the seismic risk of pipe failure should consider the aggregated effects of these two strain components. The formula to calculate the seismic risk are given in Equations (8) and (9). Note that the indices i and j in the discrete form of Equation (8) stand for discretized fault displacements and pipe-fault crossing angles (α) ranging from 1 to n and 1 to m, respectively.

$$\begin{aligned} \lambda_{failure} &= \int_D \int_\alpha P(F \mid \varepsilon_t \& \varepsilon_c\ (d,\alpha,\boldsymbol{\theta})\ )\ f_D\ (d)\ f_A\ (\alpha) d(d) \mathrm{d}(\alpha) \\ &= \sum^{n}_{i=1} \sum^{m}_{j=1} P\ (F \mid \varepsilon_{tij}\ \& \varepsilon_{cij}\ (d_i,\ \alpha_j,\ \boldsymbol{\theta}))\ \Delta\ (\upsilon_{di})\ P\ (\alpha_j) \end{aligned} \tag{8}$$

$$P(F \mid \varepsilon_t \& \varepsilon_c (d,\alpha,\boldsymbol{\theta})) = 1 - \{1 - P(F_t \mid \varepsilon_t (d,\alpha,\boldsymbol{\theta}))\} \cdot \{1 - P(F_c \mid \varepsilon_c (d,\alpha,\boldsymbol{\theta}))\} \quad (9)$$
$$= P(F_t \mid \varepsilon_t (d,\alpha,\boldsymbol{\theta})) + P(F_c \mid \varepsilon_c (d,\alpha,\boldsymbol{\theta})) - P(F_t \mid \varepsilon_t (d,\alpha,\boldsymbol{\theta})) \cdot P(F_c \mid \varepsilon_c (d,\alpha,\boldsymbol{\theta}))$$

In the above equations, $\lambda_{failure}$ is total annual rate of pipeline failure at the fault crossing. The term $P(F|\boldsymbol{\varepsilon}_t \& \boldsymbol{\varepsilon}_c(d,\alpha,\boldsymbol{\theta}))$ represents the probability of pipeline failure due to tensile ($\boldsymbol{\varepsilon}_t$) and compressive ($\boldsymbol{\varepsilon}_c$) strains developed along the pipe at the fault crossing. $P(F_t|\boldsymbol{\varepsilon}_t(d,\alpha,\boldsymbol{\theta}))$ and $P(F_c|\boldsymbol{\varepsilon}_c(d,\alpha,\boldsymbol{\theta}))$ are the pipeline failure probabilities due to tensile strain ($\boldsymbol{\varepsilon}_t$) and compressive strain ($\boldsymbol{\varepsilon}_c$), respectively. The probability expressions in the risk integral represent pipe's fragility function for a certain level of pipe strain, $\boldsymbol{\varepsilon}$, that varies with the fault displacement, d, and the fault-pipe crossing angle, α (Figure 1).The vector $\boldsymbol{\theta}$ in the fragility function describes the parameters (e.g., pipe buried depth, pipe diameter to thickness ratio and, D/t, etc.) that can affect pipe's seismic response. The probability distributions of fault displacement and fault-pipe crossing angle are represented by $f_D(d)$ and $f_A(\alpha)$. The probability distribution of α is characterized by truncated normal distribution. It maps the uncertainties in pipe-fault crossing angle due to fault rupture complexities and deficiencies in fault mapping (variations from α to α' as shown in Figure 1). The fault displacement probability is the derivative of PFD hazard curve, $\lambda_D(d)$ (i.e., $d\frac{\lambda(d)}{d(d)}$). It represents the mean annual number of events producing fault displacement exactly equal to a given displacement, d.

3. Probabilistic seismic PFD hazard and risk

The application of the methodology described in Section 2 is shown in this section. The PFD hazard is represented by two strike-slip fault scenarios having (1) a slip rate of 15 mm/year with characteristic magnitudes distributed uniformly between Mw 7.0 and Mw 7.5 (Scenario 1) and (2) a slip rate of 20 mm/year with a uniform characteristic magnitude distribution between Mw 7.5 and Mw 8.0 (Scenario 2). Scenarios 1 and 2 can represent moderate-to-high seismicity in active fault zones (e.g., East Anatolian and North Anatolian faults). The uncertainties due to fault mapping are reflected on to the calculations by assuming approximate mapped fault accuracy conditions. We also assumed the pipe crossing the fault at the middle of the ruptured fault segment. Probabilistic PFD hazard is computed by running 40,000 MC simulations that use 100-year catalog interval in each run (a total of 4×10^6 years). This routine is implemented throughout this study as it would yield reliable PFD for annual exceedance rates up to 10^{-4}. The reader is referred to Akkar and Cheng [23] as well as references cited in that paper for a broader discussion on number of MC simulations vs. reliability of hazard estimations. The resulting hazard curves of fault displacements at the center of the fault on the mapped fault (fault distance = 0m) for the two earthquake scenarios are shown in Fig. 1a, along with the hazard curves on the sites at distance (i.e., 50m, 100m and 150m) from the mapped fault (namely, fault distance).

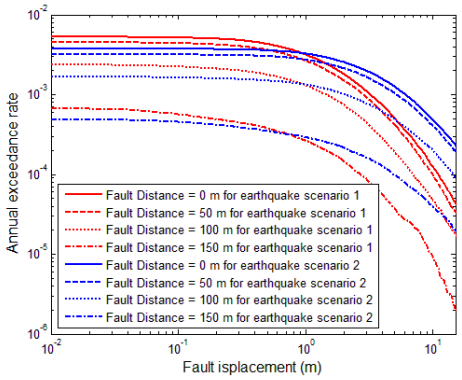

Fig. 3 Seismic hazard curves: annual exceedance rate of fault displacement for sites at different fault distances over the mapped fault (fault distance: 0, 50, 100 and 150m) for earthquake scenario 1 and 2.

The implications of PFD hazard in seismic design and vulnerability of continuous pipelines are discussed in the following. We implement the probabilistic risk integral given in Equations (8) and (9). The cases studies

consider continuous pipelines casted from S450 steel featuring an external diameter D of 36in (~0.91m) with four different wall thicknesses t, namely 1/4in (~6.4mm), 3/8in (~9.5mm), 1/2in. (~12.7mm) and 5/8 in (~15.9mm). Accordingly, the corresponding diameter-to-thickness ratios, D/t, are equal to 144, 96, 72, and 57.6, respectively. The considered material and pipe sizes cover a wide range of oil and gas transmitting continuous pipelines and would be helpful to generalize our discussions on pipeline seismic risk. The case studies in this section also consider four different buried pipe depths (i.e., 1m, 1.5m, 2m and 3m) to consider the effects of different types of soil conditions on the continuous pipeline risk.

4.1 Pipeline strain states

We use the analytical method in Karamitros et al. [17] to calculate strains along the pipeline at the fault crossings. The steel type and pipe sizes for strain calculations are already presented in Table 1. The interaction between pipe and surrounding soil (mimicked either as dense sand, soft or stiff clay soils) is modeled with bilinear elastoplastic springs [9, 25]. The spring properties of each soil type that vary as a function of buried pipe depth (*H*).

Table 1. Key parameters and corresponding values for probabilistic continuous pipeline risk assessment due to PFD

Parameter	**Considered values**
Seismic activity	Characteristic earthquake recurrence model Scenario 1: Mw 7.0 - Mw 7.5, $\dot{s}$= 15 mm/year (EAF) Scenario 2: Mw 7.5 - Mw 8.0, $\dot{s}$ = 20 mm/year (NAF)
Rupture location uncertainty	Fault-pipe crossing angles ranging between $10^o \leq \alpha \leq 90^o$ having 2σ truncated Normal distribution with $\sigma = 2.5^o$ and 5^o
Mapping accuracy	Two-sided normal distribution with σ = 43.82m
Ratio of pipe diameter to wall thickness (*D/t*)	144; 96; 72; and 57.6
Buried pipe depth	1m; 1.5m; 2m; and 3m
Soil conditions surrounding the buried pipes	Sand: friction angle=36^o, cohesion= 0kPa Soft clay: friction angle=0^o, cohesion= 50kPa Stiff clay: friction angle=0^o, cohesion = 200kPa

4.2 Pipe failure fragility

The continuous pipeline fragilities developed in this paper relate failure probability to different levels of tensile and compressive strains (i.e., P[failure|$\varepsilon(d,\alpha,\boldsymbol{\theta})$]). Assuming lognormal distribution, the failure fragilities are fitted over the empirical data discussed in the subsequent paragraphs. We adopted minimization of the sum of squared errors method [26] for fitting fragility functions.

The tensile strains of 3% and 10% that correspond to 10% and 90% failure probability [27] are used while deriving the fragility for tension failure. These deformation rates and corresponding failure probabilities are meaningful for steel pipelines with good-quality girth welds. The left tail (lower end) of lognormal tension fragility is constrained to yield no-failure at 1% tensile strain. The resulting fragility function is given in Figure 4.a.

The development of pipeline fragility for compressive stains is more complicated because failure probability due to compression is a function of *D*/*t* ratio. Wijewickreme et al. [27] assume that compressive strains corresponding to 10% and 90% failure probability are equal to 0.4/(*D/t*) and 2.4/(*D/t*), respectively. The theoretical commencement of local wrinkling (1.25% compressive strain) is in between 0.4/(*D/t*) and 2.4/(*D/t*).

We used an additional constrain that assigns no-failure for compressive strains below 0.13/(*D*/*t*) to control the left tail of compression fragilities. The resulting fragility surface for pipeline failure due to compression is given in Figure 4.b for a set of *D*/*t* values. Table 2 lists the logarithmic means (θ) and standard deviations (β) of fitted lognormal failure fragilities for tension and compression. The ones for compression failure are presented for four *D*/*t* values that are developed in this study. These values will be used to calculate the probabilistic pipeline seismic risk in the following subsection.

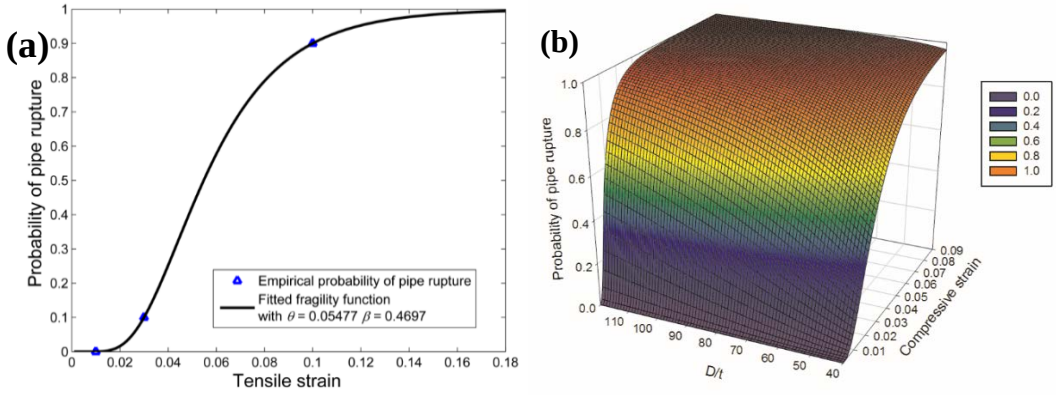

Fig. 4 Pipeline fragility for (a) tension failure and (b) compression failure

Table 2. Logarithmic means and standard deviations of pipeline fragilities against tension and compression failures

Failure state	***D/t***	***θ***	***B***
Tension	-	0.05477	0.4697
Compression	57.6	0.0170	0.6987
Compression	72	0.0136	0.6987
Compression	96	0.0102	0.6987
Compression	144	0.0068	0.6987

4.3 Pipe failure risk

The first case study discusses the significance of pipe-fault crossing angles on pipeline risk. Earthquake scenario 1 is used to represent the seismic hazard. Figure 8 shows the annual failure rates (λ) for a pipeline buried at a depth of 1m under dense sand. The annual failure rates are computed for different α associated with the uncertainty in α to manifest the inherent complications during the fault rupture process. The inaccuracy in fault-pipe crossing angle is modeled by a truncated normal probability with alternative standard deviations of 2.5° and 5°. The plots display the results for two *D*/*t* ratios (*D*/*t* = 57.6 and D/*t* = 72) to emphasize the level of change in pipeline failure rates with changes in pipeline dimensions. The tensile strain is constrained to 5% to acknowledge modeling limitations in Karamitros et al. [17]. (See discussions on the limitations of Karamitros et al. [17] analysis method in the previous sections). The comparative plots show smaller failure rates (i.e., lesser probability of failure) with increasing α for pipe-fault crossing angles up to ~ 75°. This trend reverses and pipelines are exposed to higher failure probability for $\alpha >$ ~ 70°-75°. As discussed in the previous section, the reversed trend in pipeline failure probability towards larger α may be the result of over conservative computation of curvature that affects the accuracy of tensile and compressive pipe strains. To this end, the computed pipe failure rates of α greater than approximately 70°-75° may have serious limitations and should be evaluated with some caution. We also note that the mere consideration of tensile failure would underestimate the pipe failure risk towards larger pipe-fault crossing angle. This observation is in line with our assertion about the

simultaneous consideration of tensile and compression strains in failure risk assessment of continuous pipelines. Needless to say, larger pipe dimensions reduce the pipe failure probability. Consideration of uncertainty in pipe-fault crossing angle icresaes the pipe failure probability towards large α values.

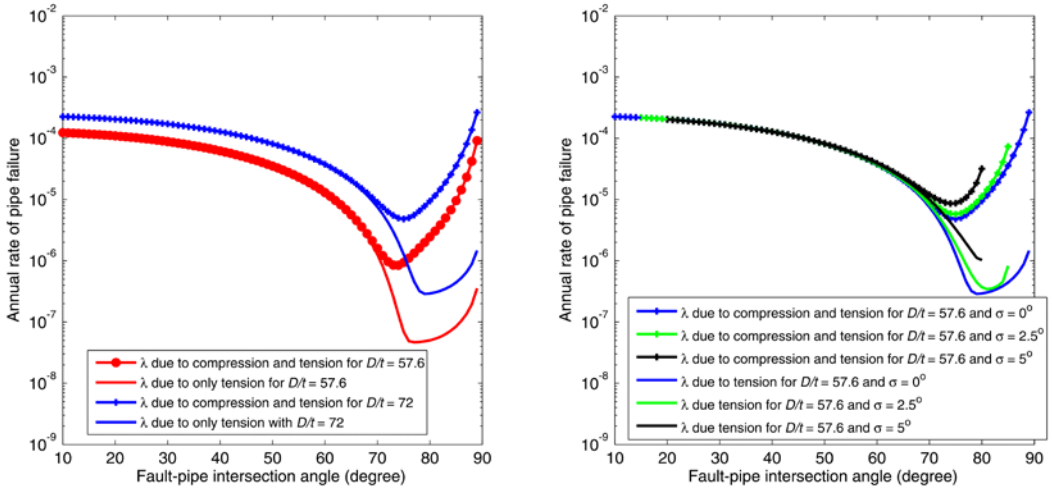

Fig. 5. Annual failure rates of pipelines in terms of pipe-fault crossing angles and the effect of pipe dimensions and uncertainty in pipe-fault crossing angle on pipe failure risk.

Figure 6 displays the annual pipe failure rates under Scenario 1 and 2 earthquakes for a fault-pipe crossing angle of 60° and a pipe buried depth of 1m under different soil conditions. Therefore, this case study discusses the effects of soil as well as earthquake activity on the seismic vulnerability of continuous pipelines. The pipeline section is represented by D/t = 57.6 in the analysis. The presented annual failure rates advocate that pipelines surrounded by stiff clays run larger failure risks with respect to soft clay and sandy soils. The pipe failure probability is inherently higher under the second earthquake scenario although earthquake Scenario 1 would also lead to a serious pipeline failure risk regardless of soil type surrounding the pipeline. To this end, seismic activity after a certain level in earthquake prone regions would always yield high risk in continuous pipeline failure under PFD demand. In passing, we note that the fictitious pipeline discussed in Figure 6 would be exposed to higher pipe failure risk for larger pipeline buried depths. This is shown in Figure 7 that displays the variation of pipe failure rate in terms of pipe buried depth when seismic hazard is represented by earthquake Scenario 1. The pipe cross-section is the same as the one used in Figure 6.

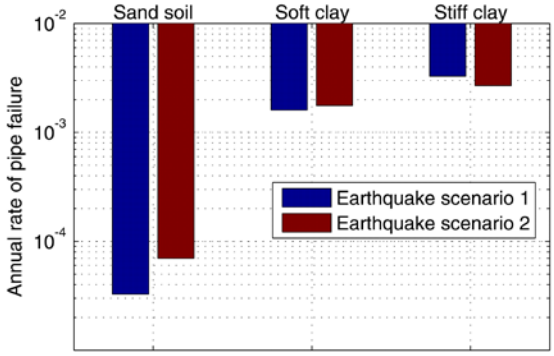

Fig. 6 Effect of soil type and earthquake activity on pipeline failure risk.

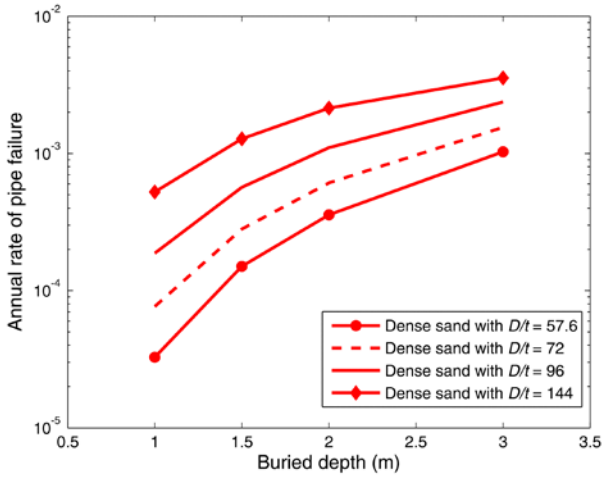

Fig.7 Variation of pipeline failure risk as a function of pipe buried depth. The results are developed for earthquake Scenario 1 under several D/t values used throughout the paper.

5. Conclusion

This paper discuses probabilistic hazard and risk assessment of continuous pipelines for PFD. The probabilistic PFD hazard has already been discussed in the literature but, to our knowledge, the probabilistic continuous pipeline risk is discussed to this extent for the first time. We used MC simulations for the probabilistic PFD hazard to account for uncertainties resulting from fault mapping accuracy and fault rupture complexity. The probabilistic risk is computed through discretized risk integral and accounts for the uncertainty in fault-pipe crossing angle due to intrinsic complexities taking place during rupture process.

The probabilistic PFD hazard results of this study emphasize the significance of pipe-fault crossing location, the corresponding angle as well as complexities arising from physical earthquake process. These phenomena are currently addressed by ad-hoc deterministic approaches in the pipeline design codes with the implementation of empirical expressions that estimate an average PFD for a particular magnitude. Our probabilistic pipeline risk case studies also advocate the difficulty in deterministic assessment of failure in continuous pipelines as it depends on the cumulative effects of variations in pipe-fault crossing angle and associated uncertainties stemming from fault rupture, pipeline buried depth and soil conditions surrounding the pipeline. These complexities together with the uncertainties in PFD hazard may result in a non-uniform risk for pipelines designed in accordance with the current pipeline design provisions. In essence, they may fail to comply with the desired performance level under seismic actions. The performance-based earthquake design in current building codes have started to define risk-targeted earthquake demands and provide performance targets in accordance with the risk-targeted demand levels [28-29]. Such a rational can also be adopted for pipeline design and discussions in this paper partially address how this objective can be achieved.

6. Acknowledgements

This paper is based on the research under the framework of STREST project (Harmonized approach to stress tests for critical infrastructures against natural hazards) that is funded by the European Union's Seventh Framework Programme under grant agreement no. 603389. The authors thank Dr. Mark Petersen and Dr. Rui Chen for explaining the case study in Petersen et al. [21] and sharing their probabilistic fault displacement hazard assessment codes for the validation of our methodology. Prof. Karamitros kindly discussed with us the essentials of the Karamitros et al. [17] analysis procedure.

7. References

[1] McGuire RK (1988): Seismic risk to lifeline systems: critical variables and sensitivities. *Proceedings of 9th World Conference on Earthquake Engineering*, Tokyo-kyoto, Japan.

[2] Mashaly E-SA and Datta TK (1989): Seismic risk analysis of buried pipelines. *Journal of transportation engineering*, **115**(3): 232-52.

[3] Pineda-Porras OA, Ordaz M (2012): Seismic Damage Estimation in Buried Pipelines Due to Future Earthquakes-The Case of the Mexico City Water System. *Earthquake-Resistant Structures-Design, Assessment and Rehabilitation*-Chapter 5. INTECH Open Access Publisher.

[4] Omidvar B, Eskandari M, Peyghaleh E (2013): Seismic damage to urban areas due to failed buried fuel pipelines case study: fire following earthquake in the city of Kermanshah, Iran. *Natural Hazards*, **67**(2):169-92.

[5] Esposito S, d'Onofrio A, Santo A, Cavalieri F, Franchin P (2015): Simulation-Based Seismic Risk Assessment of Gas Distribution Networks. *Computer-Aided Civil and Infrastructure Engineering*, **30**(7): 508-523.

[6] Mousavi M, Hesari M, Azarbakht A (2014): Seismic risk assessment of the 3rd Azerbaijan gas pipeline in Iran. *Natural Hazards*, **74**(3):1327-48.

[7] Katayama T, Kubo K, Sato N (1975): Earthquake Damage to Water and Gas Distribution Systems. *Proceedings of the U.S. National Conference on Earthquake Engineering*, Oakland.

[8] O'Rourke T, Jeon S (1999): Factors Affecting the Earthquake Damage of Water Distribution Systems. *Proceedings 5th U.S. Conference on Lifeline Earthquake Engineering*, Seattle.

[9] American Lifelines Alliance (ALA) (2001): Seismic Fragility Formulations for Water Systems, Part 1–Guideline.

[10] FEMA (Federal Emergency Management Agency) (2004): *Multi-hazard loss estimation methodology-earthquake model: HAZUS MR4 technical manual*, Washington DC.

[11] O'Rourke M (2009): Analytical Fragility Relations for Buried Segmented Pipe, *Proc. of TCLEE 2009, Lifeline Earthquake Engineering in a Multihazard Environment*, Oakland.

[12] O'Rourke M, Filipov E, Uçkan E (2014): Towards Robust Fragility Relations for Buried Segmented Pipe in Ground Strain Areas. *Earthquake Spectra*, doi: http://dx.doi.org/10.1193/032311EQS076M,

[13] Datta TK (1999): Seismic response of buried pipelines: a state-of-the-art review. *Nuclear Engineering and Design*, **192**(2-3): 271-284.

[14] Vazouras P, Karamanos SA, Dakoulas P (2010): Finite element analysis of buried steel pipelines under strike-slip fault displacements. *Soil Dynamics and Earthquake Engineering*, **30**(11):1361–76.

[15] Vazouras P, Karamanos SA, Dakoulas P (2012): Mechanical behavior of buried steel pipes crossing active strike-slip faults. *Soil Dynamics and Earthquake Engineering*, **41**:164-80.

[16] Karamitros DK, Bouckovalas GD, Kouretzis GP, Gkesouli V (2011): An analytical method for strength verification of buried steel pipelines at normal fault crossings. *Soil Dynamics and Earthquake Engineering*, **31**(11): 1452-1464.

[17] Karamitros DK, Bouckovalas GD, Kouretzis GP (2007): Stress analysis of buried steel pipelines at strike-slip fault crossings. *Soil Dynamics and Earthquake Engineering*, **27**(3): 200-211.

[18] Uckan E, Akbas B, Shen J, Rou W, Paolacci F, O'Rourke M (2015): A simplified analysis model for determining the seismic response of buried steel pipes at strike-slip fault crossings. *Soil Dynamics and Earthquake Engineering*; **75**:55-65.

[19] Stepp JC, Wong I, Whitney J, Quittmeyer R, Abrahamson N, Toro G, Youngs R, Coppersmith K, Savy J, Sullivan T (2001): Yucca Mountain PSHA Project Members. Probabilistic seismic hazard analyses for ground motions and fault displacement at Yucca Mountain, Nevada. *Earthquake Spectra*, **17**:113–150.

[20] Youngs RR, Arabasz WJ, Anderson RE, Ramelli AR, Ake JP, Slemmons DB, et al. (2003): A methodology for probabilistic fault displacement hazard analysis (PFDHA). *Earthquake Spectra*, **19**(1):191-219.

[21] Petersen MD, Dawson TE, Chen R, Cao T, Wills CJ, Schwartz DP, Frankel AD (2011): Fault displacement hazard for strike-slip faults. *Bulletin of the Seismological Society of America*, **101**(2): 805-825.

[22] Wells DL, Coppersmith KJ (1994): New empirical relationships among magnitude, rupture length, rupture width, rupture area, and surface displacement. *Bulletin of the Seismological Society of America*, **84**(4): 974–1002.

[23] Akkar S, Cheng, Y (2015): Application of a Monte-Carlo simulation approach for the probabilistic assessment of seismic hazard for geographically distributed portfolio. *Earthquake Engineering and Structural Dynamics*, **45**(4): 525–541.

[24] McGuire RK (2004): *Seismic Hazard and Risk Analysis*, Earthquake Engineering Research Institute: Oakland, CA.

[25] American Lifeline Alliance (ALA) (2005): Design Guidelines for Seismic Resistant Water Pipeline Installations. *Report FEMA, NIBS and ALA 2005/03*. G&E Engineering Systems Inc.

[26] Baker JW (2015): Efficient Analytical Fragility Function Fitting Using Dynamic Structural Analysis. *Earthquake Spectra*, **31**(1):579-99.

[27] Wijewickreme D, Honegger D, Mitchell A, Fitzell T (2005): Seismic vulnerability assessment and retrofit of a major natural gas pipeline system: A case history. *Earthquake Spectra*, **21**(2):539-67.

[28] Luco N, Ellingwood BR, Hamburger RO, Hooper JD, Kimball JK, Kircher CA (2007): Risk-Targeted versus Current Seismic Design Maps for the Conterminous United States. *Proceedings of the Structural Engineers Association of California 76th Annual Convention*, Squaw Creek.

[29] Luco N, Gerstenberger MC, Uma SR, Ryu H, Liel AB, Raghunandan M (2011): A methodology for post-mainshock probabilistic assessment of building collapse risk. *Proceedings of the Ninth Pacific Conference on Earthquake Engineering Building an Earthquake-Resilient Society*, Auckland, New Zealand.